Coherent Transfer of Transverse Optical Momentum to the Motion of a Single Trapped Ion

Felix Stopp,[1] Maurizio Verde,[1] Milton Katz,[2] Martin Drechsler,[2,3]
Christian T. Schmiegelow,[2,3,*] and Ferdinand Schmidt-Kaler[1]
[1]QUANTUM, Institut für Physik, Universität Mainz, Staudingerweg 7, 55128 Mainz, Germany
[2]Universidad de Buenos Aires, Facultad de Ciencias Exactas y Naturales, Departamento de Física, Buenos Aires, Argentina
[3]CONICET—Universidad de Buenos Aires, Instituto de Física de Buenos Aires (IFIBA), Buenos Aires, Argentina

(Received 4 July 2022; revised 28 October 2022; accepted 22 November 2022; published 23 December 2022)

Using a structured light beam carrying orbital angular momentum, we demonstrate excitation of the center-of-mass motion of a single atom in the transverse direction to the beam's propagation. This interaction enables quantum control of atomic motion in all axes with a single beam direction, which leads to applications in quantum computing and simulations with ion crystals. Here we demonstrate all the key features required for these applications, namely, coherent dynamics and strong carrier suppression in a configuration with the ion centered in the beam, which allows for single ion addressing and also provides robustness against pointing instabilities. To quantify transverse momentum transfer, we observe coherent dynamics on the sidebands of the $S_{1/2}$ to $D_{5/2}$ transition near 729 nm of a singly charged $^{40}Ca^{+}$ ion, cooled near the ground state of motion in the 3D harmonic potential of a Paul trap, and placed at the center of a first-order Laguerre-Gaussian beam. Exchange of quanta in the perpendicular direction to the beam's wave vector $\boldsymbol{k}$ is observed with a centered vortex shaped beam, together reduction of the parasitic carrier excitation by a factor of 40. This is in sharp contrast to the vanishing spin-motion coupling at the center of the Gaussian beam. Further, we characterize the coherent interaction by an effective transverse Lamb-Dicke factor $\eta_{\perp}^{\mathrm{exp}} = 0.0062(5)$ which is in agreement with our theoretical prediction $\eta_{\perp}^{\mathrm{theo}} = 0.0057(1)$.

DOI: 10.1103/PhysRevLett.129.263603

Light can transfer both linear and angular momentum to massive particles. The angular momentum of a light beam is determined not only by its polarization, but also by its spatial structure. For example, vortex beams such as Laguerre-Gaussian beams have been shown to carry orbital angular momentum (OAM), associated with their spatial structure [1]. Since then, the use of structured beams has become a commonly applied technique for imaging, communications, optical manipulation mechanics [2], and control and manipulation of cold atomic gases [3]. After the pivotal work in 1995 by Rubensztein-Dunlop and her team, showing that trapped micron-sized particles could be set to rotate with the sense sign of the beam's singularity [4], various kinds of platforms have been used to prove light's orbital angular momentum transfer to classical objects [5,6] and to cold atomic gases [3,7]. Following these ideas into the single atom quantum regime, here we show that the angular momentum coming from the beam's structure can coherently excite the center-of-mass motion of a trapped ion. In particular, we show that, when placed at the center of a vortex beam, the ion can be coherently driven in the plane perpendicular to the incident direction. This strikingly contrasts with the cases where the plane wave approximation holds and transversal momentum exchange is not possible, such as in the case of the center of Gaussian beams.

Here, we use a single trapped ion which can be positioned with nanometer precision with respect to a structured beam [8]. After laser cooling of the motion, the ion's center of mass dynamics can be adequately described as a three-dimensional quantum harmonic oscillator [9]. Then, on a narrow hertz-wide electric quadrupole transition, the internal electronic and external vibrational quantum states of the ion can be prepared, manipulated, and read out via coherent driving in the resolved sideband regime [10]. These prerequisites allow for pushing the seminal experiments where light's orbital angular momentum can be transferred to the motion of a single trapped particle to the quantum regime. In a previous experiment, we showed that orbital angular momentum can be transferred to the valence electron of an ion [11]. Interestingly, such a transfer is also possible for the external motional degrees of freedom. For example, when an ion is placed at the side of a Gaussian beam, spatial gradients can excite motion transversely to the beam's propagation direction [12]. However, using a misaligned Gaussian beam necessarily leads to problems with respect to pointing stability, single ion addressing, as well as ac Stark shift and carrier suppression, hindering its applicability for quantum control. Here, we overcome these limitations and demonstrate coherent driving of the ion's transverse center-of-mass motion by using a vortex beam with a field null at the

center, where the ion is aligned. Moreover, we show a strong suppression of parasitic carrier transition—the excitation without change in motion—when the ion is at the center of the vortex beam. These are all the prerequisites needed to achieve addressed quantum gates and cooling or thermometry on modes transverse to the laser's propagation direction.

We start by briefly presenting the fundamental equations that determine the possible interaction terms for a structured beam to show that it can transfer its orbital angular momentum to a single trapped ion [13]. The quadrupole term of the light-matter interaction Hamiltonian reads [14–16]

$$\hat{H} \sim \sum_{i,j} \hat{q}_i \hat{q}_j \frac{\partial E_j^{(+)}}{\partial q_i}\bigg|_{\hat{Q}_i} e^{-i\omega t} + \text{H.c.}, \tag{1}$$

where $\hat{q}_i = \{\hat{x}, \hat{y}, \hat{z}\}$ are the position operators pertaining to the valence electron, q_i are the coordinates of the electric field components E_j with angular frequency ω and the $\hat{Q}_i = \{\hat{X}, \hat{Y}, \hat{Z}\}$ are operators acting on the ion's center-of-mass coordinates. We consider a beam traveling in the $\boldsymbol{e}_z$ direction at 45° to respect of both radial trap coordinates $\{r_{R1}, r_{R2}\}$ and orthogonal to the axial trap direction $r_{ax} = x$ as shown in Figs. 1(a) and 1(b).

For the case of a traveling wave, as in the center of a Gaussian beam, the electric field being $\boldsymbol{E}^{(+)}_{\text{Gauss}} \sim E_0(\boldsymbol{e}_x + \sigma i \boldsymbol{e}_y)\exp(ikz)$ with circular polarization $\sigma = \pm 1$ and wave number k, one obtains the usual quadrupole transition selection rules for the valence electron [17,18]. The sideband transitions are governed by the term $\hat{H}_{\text{Gauss}} \sim \exp\{ik\hat{Z}\}$. Since $\hat{Z} = (\hat{R}_{R1} - \hat{R}_{R2})/\sqrt{2}$ only projects on the radial eigendirections of the ion's motion, radial sidebands are excited, while axial ones are forbidden, being orthogonal to $\boldsymbol{k}$, see Figs. 1(a) and 1(c). The coupling strength of these transitions will be governed by a longitudinal Lamb-Dicke parameter $\eta_{\parallel} = kr_0$, with $r_0 = \sqrt{\hbar/2m\omega_{1,2}}$ for a quantum harmonic oscillator, being m the mass of the ion and $\omega_{1,2}$ the secular frequencies in the radial directions r_{R1} and r_{R2}. Thus, at the center of a Gaussian beam, sideband transitions are driven by the longitudinal electric field gradient, strictly oriented along the propagation direction $\boldsymbol{k}$.

The situation is entirely different for a vortex beam carrying OAM, where transverse electric field gradients, perpendicular to the propagation direction, can also mediate sideband excitations, as show in Figs. 1(b) and 1(d). At its center, the electric field of a Laguerre-Gaussian beam is $\boldsymbol{E}^{(+)}_{\text{LG}} \sim E_0\sqrt{2}w_{\text{LG}}^{-1}(\boldsymbol{e}_x + i\sigma\boldsymbol{e}_y)\exp(ikz)(x + ily)$, with waist w_{LG} where the intensity drops to $1/e^2$, $l = \pm 1$ units of orbital angular momentum and $\sigma = \pm 1$ units of intrinsic angular momentum. Upon evaluating the interaction Hamiltonian for this field using Eq. (1), one can sort the result in two terms. The first one contains the coordinates

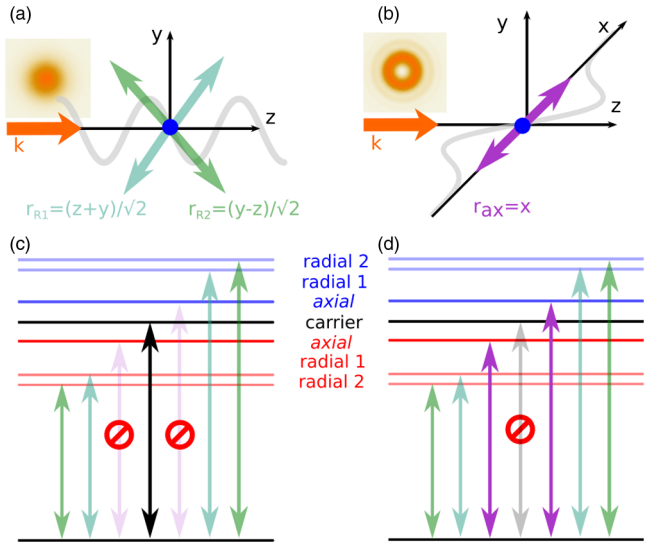

FIG. 1. Intensity profile and wave vector $\boldsymbol{k}$ (orange) traveling along the z direction for (a) a Gaussian beam and (b) an OAM-carrying vortex beam. Correspondingly in (c) and (d) the energy levels and possible motional transitions for each beam, on a subspace where the magnetic number changes in $\Delta m = \pm 1$. In (a), for the Gaussian beam, the longitudinal variation of the traveling wave (gray sinusoidal) can only drive transitions with projection along the beam's z direction, i.e., in the ion's radial directions r_{R1} (green) and r_{R2} (cyan). Consequently transitions, shown in (c), will be allowed for the carrier and the radial sidebands, while axial sidebands will be forbidden, due to the orthogonality of the wave vector $\boldsymbol{k}$ with respect to the ion's axial direction r_{ax} (purple). Conversely in (b), for the OAM-carrying vortex beam, the transverse variation of the beam's intensity (gray curve) lies in its x-y plane and can now drive transitions in the ion's axial r_{ax} direction. Here, as shown in (d), the carrier is forbidden but the axial sideband, which lies transversal to be beam's propagation direction is now allowed. Indeed, both axial and radial sideband modes are excited, because of their non-vanishing projection onto the transversal x-y plane.

pairs of the transverse directions $\{xx, xy, yx, yy\}$ and accounts for two units of angular momentum of the beam being transferred to its valence electron, as has been demonstrated [11]. Here, the coupling to the external vibrational degrees of motion to the light field is identical as for a Gaussian beam: only sideband excitations in the direction parallel to $\boldsymbol{k}$ are allowed.

The second term, that contains the crossed longitudinal-transverse coordinate pairs $\{xz, yz\}$, reads

$$\hat{H}^{\perp}_{\text{LG}} \sim \exp\{ik\hat{Z}\}\frac{\sqrt{2}}{w_{\text{LG}}}(\hat{X} + i\hat{Y}). \tag{2}$$

This Hamiltonian has a linear dependence on the position operators $\hat{X} = \hat{R}_{ax}$ and $\hat{Y} = (\hat{R}_{R1} + \hat{R}_{R2})/\sqrt{2}$. This results in coupling to all the eigendirections of the trap, now enabling the axial sideband transition, corresponding to motion transverse to the beam's propagation direction.

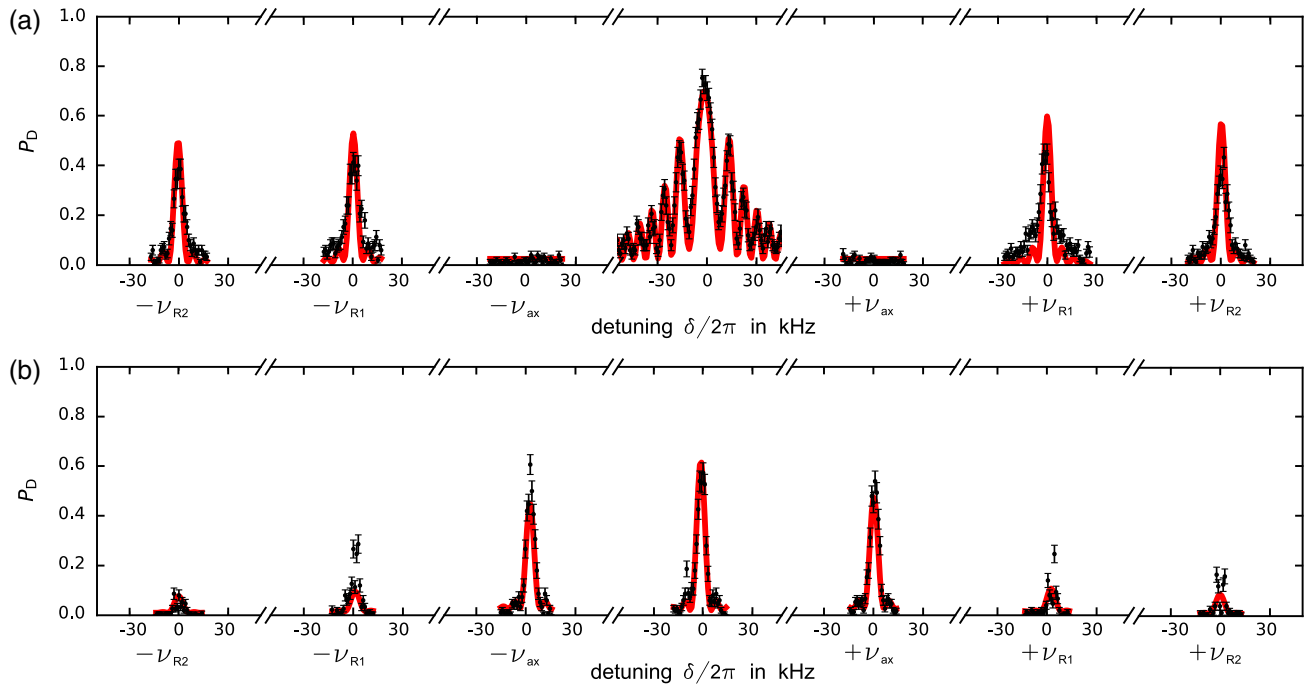

FIG. 2. Spectrum of the transition $|S_{1/2}, m_J = -1/2\rangle \leftrightarrow |D_{5/2}, m_{J'} = -3/2\rangle$ with (a) a Gaussian beam and (b) a vortex beam. The graph shows the dark state population P_D for the carrier, axial sidebands ($\delta = \pm 2\pi\nu_{ax}$), and radial sidebands ($\delta = \pm 2\pi\nu_{R1,R2}$). Black dots depict our measurements in frequency steps of $\Delta\nu = 1$ kHz, while the red continuous lines map numerical calculations (based on Eq. (6) of the supplementary material). The selected fixed values for the calculations are taken from our pulsed laser beam parameters: $P_{LG} = 10$ μW, $P_{Gauss} = 310$ nW, $w_{Gauss} = 2.8$ μm, $w_{LG} = 3.3$ μm, and $\tau = 150$ μs, as well as values for Doppler-cooled ion: $\langle n_{ax}\rangle = 15$, $\langle n_{R1,R2}\rangle = 7$.

Moreover, the carrier excitation is vanishing, resembling what happens in a standing wave [19], where either carrier or first sidebands along the direction of the beam have been suppressed by placing a single ion on its nodes or antinodes [20].

The strength of the transverse sideband, in the vortex beam center, is governed by a *transverse* Lamb-Dicke parameter $\eta_\perp = \sqrt{2}x_0/w_{LG}$, which now depends on the beam waist w_{LG} and by the spatial wave packet spread x_0 in the axial direction $r_{ax} = x$. This describes a quadrupole excitation of the valence electron, changing its magnetic number by $\Delta m = \pm 1$, together with an excitation of the external degree of freedom which can acquire or give a phonon $\Delta n_{ax} = \pm 1$. The excitation of a transversal motional degree is enabled by the crosswise spatial gradient of the beam, as illustrated in Figs. 1(b) and 1(d), while the change in internal angular momentum Δm is determined by its polarization.

To demonstrate this anomalous momentum transfer, we use an experimental setup where a single $^{40}Ca^+$ ion is confined in an harmonic potential of quadruple trap mounted in a UHV chamber [21]. We use a radio-frequency Paul trap producing a radial harmonic confinement with secular frequencies of $\omega_{R1,R2} = 2\pi \times (1.70, 2.05)$ MHz. The axial confinement is generated by an electrostatic potential, yielding an axial secular frequency of $\omega_{ax} \simeq 2\pi \times 700$ kHz, corresponding to a ground state wave packet size of $r_{0,ax} = 15$ nm. The ion is Doppler cooled in all three trap axes using the dipole transition $4S_{1/2} \leftrightarrow 4P_{1/2}$ close to 397 nm with an additional 866 nm repump laser to form a closed cooling cycle. Single ion imaging is achieved on an EMCCD camera, by collecting the laser-induced fluorescence through an objective with numerical aperture NA = 0.3 and focal distance of 66.9 mm, which leads to a diffraction limited image with magnification $M = 15.6(5)$.

The setup is equipped with two 729 nm laser beams to drive the $4S_{1/2} \leftrightarrow 3D_{5/2}$ quadrupole transition. A preparation beam, with a Gaussian shape and $\boldsymbol{k}$-vector projection onto all three trap axes is used to initialize the ion in the ground state $|S_{1/2}, m_J = -1/2\rangle$ and for optional sideband cooling of the axial vibration mode. A second 729 nm beam is used as a probe and can be set to have either a Gaussian or a Laguerre-Gaussian transverse mode profile with a holographic pitch-fork pattern [22]. This beam is focused onto the ion though the imaging lens to a beam waist of $w_{LG} = 3.34(7)$ μm propagating perpendicular to the trap's axial direction, i.e., along z, as seen in Fig. 1. Two steering mirrors allow for the perpendicular alignment of the beam to the axial direction with a precision of $< 1°$. Moreover, the beam can be scanned across the ion with a range of ≈1 μm in all three spatial directions by using a closed-loop piezo stage. A Zeeman splitting of 5 MHz between the sublevels in the $D_{5/2}$ state is generated by a magnetic field

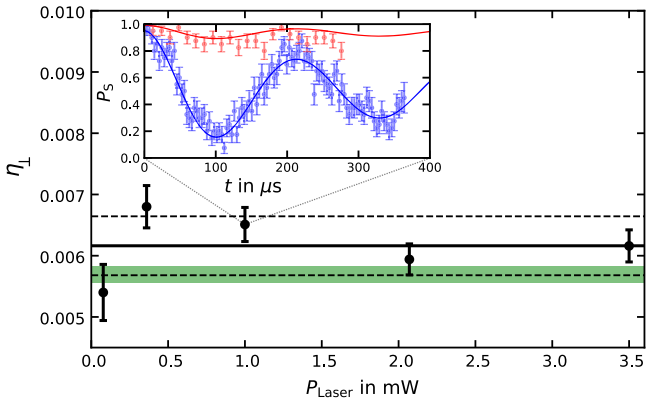

FIG. 3. Comparison of transversal Lamb-Dicke parameters determined by different methods. Points with error bars were determined by fits to red and blue oscillations of the transverse sideband, as exemplified in the inset for $P_{\text{Laser}} = 1$ mW. The black and dashed lines at $\eta_\perp^{\text{exp}} = 0.0062(6)$ show the mean value and 1σ range for all measured powers. In green, the 1σ range of the theoretically expected value of $\eta_\perp^{\text{theo}} = 0.0057(1)$ is drawn with an uncertainty which is dominated by the error in the determination of the beam waist w_{LG}.

aligned parallel to the propagation direction of the probe beam. The beam's polarization and frequency are set to drive the $\Delta m = -1$ transition $|S_{1/2}, m_J = -1/2\rangle \leftrightarrow |D_{5/2}, m_{J'} = -3/2\rangle$ [17].

We measure the resolved sideband spectra of the Gaussian and the Laguerre-Gaussian with $l = -1$ beam by scanning the probe laser frequency, see Fig. 2. An experimental sequence consists of Doppler cooling, spin initialization, pulsed excitation and state dependent fluorescence readout. For the Gaussian beam, Fig. 2(a), we observe strong coherent oscillations on the carrier, radial sidebands determined by the longitudinal Lamb-Dicke parameter and absent axial sidebands. The experimental data (black) are in good agreement with a model (red) generated by independently measured parameters. The spectra pertaining to the Laguerre-Gaussian probe beam shown in Fig. 2(b) show clearly visible axial sidebands, determined by the transverse Lamb-Dicke parameter. From the independently measured beam waist and secular frequency, we compute a transverse Lamb-Dicke parameter of $\eta_\perp^{\text{theo}} = \sqrt{2}x_0/w_{\text{LG}} = 0.0057(1)$. The difference in strength between axial and radial sidebands is explained by the projection geometry of each eigendirection onto the beam's propagation direction and from the wave packet sizes for different mode frequencies. As the transversal electric field gradients are smaller by a factor of $\sqrt{2}/kw_{\text{LG}}$ as compared to the longitudinal ones, the value of the transversal Lamb-Dicke parameter is reduced. Accordingly, we increased the laser power by a factor of 30. Note that also for the vortex beam we observe a residual carrier excitation which is reduced by a factor 40 as compared to that for a Gaussian beam shape. This is quantitatively explained by accounting for the finite wave packet spatial extension, which explores an extended region around the center of the beam and then senses an effective nonvanishing electric field intensity [8]. We stress that in all of Fig. 2 the model was not fitted to the data, but ran with independently measured parameters, see Supplemental Material [23] for details.

Next, we precisely measure the transverse Lamb-Dicke parameter $\eta_\perp^{\text{exp}}$ for the Laguerre-Gaussian beam by analyzing Rabi oscillations on the axial red and blue sidebands, see Fig. 3. The ion was cooled near to the ground state of axial motion to a mean phonon number $\langle n_{\text{ax}} \rangle = 0.19(10)$ to obtain good contrast of the sideband Rabi oscillations. From the data of the red and blue sidebands, we extract $\eta_\perp^{\text{exp}}$, using the independently measured Rabi frequency and mean phonon number as fixed parameters, by a simultaneous fit of both curves. Measurements were taken for five different beam powers between 78 μW and 3.5 mW, in order to exclude any dependence on the beam power. By averaging, we obtain a value of $\eta_\perp^{\text{exp}} = 0.0062(5)$ being in agreement with the theoretical value of $\eta_\perp^{\text{theo}} = 0.0057(1)$, all shown in Fig. 3.

Using the ion as a well-localized electrical field probe, we explore the structural dependence of the sideband and

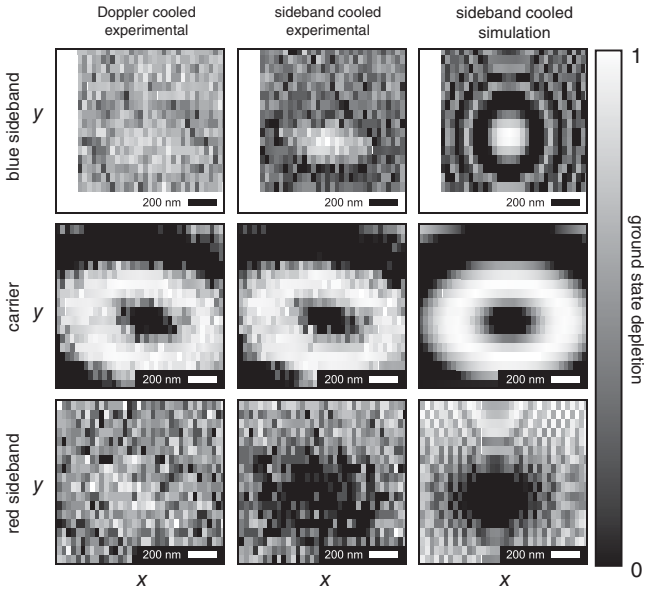

FIG. 4. Excitation profiles in x and y directions. First, second and third rows refer, respectively, to blue sideband, carrier, and red sideband of the $|S_{1/2}, m_J = -1/2\rangle \leftrightarrow |D_{5/2}, m_{J'} = -3/2\rangle$ transition. The first and second columns show, respectively, the measurements for a Doppler-cooled and a sideband-cooled ion close to the ground state. They have been obtained by scanning the vortex beam through the ion using step sizes of 32 (x) and 64 nm (y), a pulse duration of $\tau = 55$ μs, corresponding to the blue sideband's π time of the near ground-state cooled ion, and two different powers for the carrier $P_{\text{car}} = 45$ μW and the sidebands $P_{\text{sb}} = 2.8$ mW. Using the same parameters, numerical calculations for a sideband-cooled ion are shown in the third column.

the carrier transitions excited by the Laguerre-Gaussian beam. We vary the wave packet size using an ion either Doppler cooled with $\langle n_{\mathrm{ax}}\rangle \approx 15$ or alternatively, cooled close to its motional ground state in the axial direction, as shown in Fig. 4. We scan the beam over the ion in the transverse x and y directions, and record the excitation probability for an effective pulse area of about π for ground-state cooled axial blue sideband, corresponding to a rectangular pulse with a duration of 55 μs. The carrier shows a ring structure, due to the increase of the electric field amplitude radially from the beam's center [8]. Conversely, the sidebands display maximum excitation at the center of the vortex beam, due to the transversal gradient. This is observed for all cases except for the red sideband $|n_{\mathrm{ax}}\rangle \rightarrow |n_{\mathrm{ax}} - 1\rangle$ of the sub-Doppler cooled ion, where excitation is suppressed by the fact that the oscillator state is near $|n_{\mathrm{ax}} = 0\rangle$. The strongest sideband excitation is achieved on the transversal blue sideband $|n_{\mathrm{ax}}\rangle \rightarrow |n_{\mathrm{ax}} + 1\rangle$ in the dark center of the vortex beam. Moreover, we note all the sidebands exhibit a halo structure, which is caused by the off-resonant excitation of the carrier, as we verify by numerical calculations of the expected profiles, see right column in Fig. 4.

In conclusion, we demonstrated the spatial gradients at the center of a structured laser beam can be used to coherently drive center-of-mass motion modes while strongly reducing carrier modes. This technique might find various applications. For example in quantum computing with linear ion chains where addressing beams control single- and multi-qubit operations [24–26]. In order to provide adequate ion addressing, control beams have to be focused from a radial direction onto one ion in the linear crystal. Using a plane wave, this configuration only allows acting on the ion's motion along the beam's wave vector direction, i.e. the radial direction. Now, using a vortex beam one can combine single ion addressing capabilities with control over the transverse (axial) direction, allowing one to drive quantum gate operations, cooling and general motion control on the axial modes. This is beneficial as axial modes are less prone to spectral crowding as compared to radial modes [27] and are amenable to sympathetic cooling [28]. Also, the diminished parasitic carrier excitation might help reduce the overhead caused by AC Stark-shifts [29] in light mediated quantum gates and in the exploration of sideband cooling limits for trapped ions. Similarly, in planar ion crystals, as those intended for quantum simulations [30–32], one could now sense and manipulate the in-plane phonon occupation numbers locally using addressing beams impinging from the normal direction. Also, this can be beneficial for ion traps where one direction is inaccessible by lasers. Finally, we note that, by using dipolar transitions, one could observe torques and coherently manipulate single ions or ion crystals by resonant and off-resonant forces generated by the transverse field gradients of vortex beams.

We acknowledge the Deutsche Forschungsgemeinschaft within the TRR 306 (QuCoLiMa, Project-ID 429529648), the Alexander von Humboldt-Stiftung/Foundation, and the Agencia I + D + i with grant PICT 2019—4349, for financial support. We thank A. Trimeche and specially U. Poschinger for careful reading and comments on the manuscript, as well as A. Afanasev, C. E. Carlson, and G. Jacob for fruitful discussions.

F. S. and M. V. contributed equally to this work.

*schmiegelow@df.uba.ar

[1] L. Allen, M. W. Beijersbergen, R. J. C. Spreeuw, and J. P. Woerdman, Phys. Rev. A **45**, 8185 (1992).
[2] M. J. Padgett, Opt. Express **25**, 11265 (2017).
[3] L. Amico, M. Boshier, G. Birkl, A. Minguzzi, C. Miniatura, L.-C. Kwek, D. Aghamalyan, V. Ahufinger, D. Anderson, N. Andrei *et al.*, AVS Quantum Sci. **3**, 039201 (2021).
[4] H. He, M. E. J. Friese, N. R. Heckenberg, and H. Rubinsztein-Dunlop, Phys. Rev. Lett. **75**, 826 (1995).
[5] M. Padgett and R. Bowman, Nat. Photonics **5**, 343 (2011).
[6] A. B. Stilgoe, T. A. Nieminen, and H. Rubinsztein-Dunlop, Nat. Photonics **16**, 346 (2022).
[7] M. F. Andersen, C. Ryu, P. Cladé, V. Natarajan, A. Vaziri, K. Helmerson, and W. D. Phillips, Phys. Rev. Lett. **97**, 170406 (2006).
[8] M. Drechsler, S. Wolf, C. T. Schmiegelow, and F. Schmidt-Kaler, Phys. Rev. Lett. **127**, 143602 (2021).
[9] S. Stenholm, Rev. Mod. Phys. **58**, 699 (1986).
[10] D. Leibfried, R. Blatt, C. Monroe, and D. Wineland, Rev. Mod. Phys. **75**, 281 (2003).
[11] C. T. Schmiegelow, J. Schulz, H. Kaufmann, T. Ruster, U. G. Poschinger, and F. Schmidt-Kaler, Nat. Commun. **7**, 12998 (2016).
[12] A. D. West, R. Putnam, W. C. Campbell, and P. Hamilton, Quantum Sci. Technol. **6**, 024003 (2021).
[13] S. M. Barnett, J. Mod. Opt. **55**, 2279 (2008).
[14] S. Van Enk and G. Nienhuis, Europhys. Lett. **25**, 497 (1994).
[15] D. James, Appl. Phys. B **66**, 181 (1998).
[16] S. M. Barnett, F. C. Speirits, and M. Babiker, J. Phys. A **55**, 234008 (2022).
[17] C. T. Schmiegelow and F. Schmidt-Kaler, Eur. Phys. J. D **66**, 157 (2012).
[18] C. Roos, Controlling the quantum state of trapped ions, Ph.D thesis, 2000 (unpublished).
[19] C. T. Schmiegelow, H. Kaufmann, T. Ruster, J. Schulz, V. Kaushal, M. Hettrich, F. Schmidt-Kaler, and U. G. Poschinger, Phys. Rev. Lett. **116**, 033002 (2016).
[20] A. B. Mundt, A. Kreuter, C. Becher, D. Leibfried, J. Eschner, F. Schmidt-Kaler, and R. Blatt, Phys. Rev. Lett. **89**, 103001 (2002).
[21] S. Wolf, S. Richter, J. von Zanthier, and F. Schmidt-Kaler, Phys. Rev. Lett. **124**, 063603 (2020).
[22] J. Arlt, K. Dholakia, L. Allen, and M. Padgett, J. Mod. Opt. **45**, 1231 (1998).
[23] See Supplemental Material at http://link.aps.org/supplemental/10.1103/PhysRevLett.129.263603 for theoretical framework, extended experimental methods and wave packet finite spatial spread analysis.

[24] I. Pogorelov, T. Feldker, C. D. Marciniak, L. Postler, G. Jacob, O. Krieglsteiner, V. Podlesnic, M. Meth, V. Negnevitsky, M. Stadler, B. Hofer, C. Wachter, K. Lakhmanskiy, R. Blatt, P. Schindler, and T. Monz, PRX Quantum **2**, 020343 (2021).

[25] J. Hilder, D. Pijn, O. Onishchenko, A. Stahl, M. Orth, B. Lekitsch, A. Rodriguez-Blanco, M. Müller, F. Schmidt-Kaler, and U. G. Poschinger, Phys. Rev. X **12**, 011032 (2022).

[26] S. Debnath, N. M. Linke, C. Figgatt, K. A. Landsman, K. Wright, and C. Monroe, Nature (London) **536**, 63 (2016).

[27] K. A. Landsman, Y. Wu, P. H. Leung, D. Zhu, N. M. Linke, K. R. Brown, L. Duan, and C. Monroe, Phys. Rev. A **100**, 022332 (2019).

[28] J. B. Wübbena, S. Amairi, O. Mandel, and P. O. Schmidt, Phys. Rev. A **85**, 043412 (2012).

[29] H. Häffner, S. Gulde, M. Riebe, G. Lancaster, C. Becher, J. Eschner, F. Schmidt-Kaler, and R. Blatt, Phys. Rev. Lett. **90**, 143602 (2003).

[30] J. D. Arias Espinoza, M. Mazzanti, K. Fouka, R. X. Schüssler, Z. Wu, P. Corboz, R. Gerritsma, and A. Safavi-Naini, Phys. Rev. A **104**, 013302 (2021).

[31] C. Monroe, W. C. Campbell, L.-M. Duan, Z.-X. Gong, A. V. Gorshkov, P. W. Hess, R. Islam, K. Kim, N. M. Linke, G. Pagano, P. Richerme, C. Senko, and N. Y. Yao, Rev. Mod. Phys. **93**, 025001 (2021).

[32] L. Bond, L. Lenstra, R. Gerritsma, and A. Safavi-Naini, arXiv:2202.13681.